

Interpretation of Departure from the Broad Line Region Scaling in Active Galactic Nuclei

BOŻENA CZERNY,¹ JIAN-MIN WANG,² PU DU,² KRZYSZTOF HRYNIEWICZ,³ VLADIMIR KARAS,⁴ YAN-RONG LI,²
SWAYAMTRUPTA PANDA,^{1,5} MARZENA SNIEGOWSKA,^{1,6} CONOR WILDY,¹ AND YE-FEI YUAN⁷

¹*Center for Theoretical Physics, Polish Academy of Sciences, Al. Lotnikow 32/46, 02-668 Warsaw, Poland*

²*Key Laboratory for Particle Astrophysics, Institute of High Energy Physics, Chinese Academy of Sciences, 19B Yuquan Road, Beijing 100049, China*

³*Nicolaus Copernicus Astronomical Center, Polish Academy of Sciences, ul. Bartycka 18, 00-716 Warsaw, Poland*

⁴*Astronomical Institute, Academy of Sciences, Bocni II, CZ-141 31 Prague, Czech Republic*

⁵*Nicolaus Copernicus Astronomical Center (PAN), ul. Bartycka 18, 00-716 Warsaw, Poland*

⁶*Warsaw University Observatory, Al. Ujazdowskie 4, 88-478 Warsaw, Poland*

⁷*Astronomy Department, University of Science and Technology of China, Hefei 230026, China*

(Received XXXX XX, 201X; Revised XXXX XX, 201X; Accepted November 26, 2018)

Submitted to ApJ

ABSTRACT

Most results of the reverberation monitoring of active galaxies showed a universal scaling of the time delay of the H β emission region with the monochromatic flux at 5100 Å, with very small dispersion. Such a scaling favored the dust-based formation mechanism of the Broad Line Region (BLR). Recent reverberation measurements showed that actually a significant fraction of objects exhibit shorter lags than the previously found scaling. Here we demonstrate that these shorter lags can be explained by the old concept of scaling of the BLR size with the ionization parameter. Assuming a universal value of this parameter and universal value of the cloud density reproduces the distribution of observational points in the time delay-monochromatic flux plane, provided that a range of black hole spins is allowed. However, a confirmation of the new measurements for low/moderate Eddington ratio sources is strongly needed before the dust-based origin of the BLR can be excluded.

Keywords: galaxies: active – galaxies: Seyfert – quasars: emission lines – accretion, accretion disks

1. INTRODUCTION

The most prominent features in type 1 Active Galactic Nuclei (AGNs) are broad emission lines present in their spectra (for a review, see e.g. Krolik 1999). The Broad Line Region (BLR) is unresolved with current instruments but the reverberation mapping (RM) of nearby active galaxies pioneered by Liutyi (1977) and done much more intensively since the 1990' (e.g. Peterson et al. 2004; Kaspi et al. 2000; Bentz et al. 2013; Du et al. 2018) allowed to measure the size of the BLR from the time delay between the variations of emission lines and the continuum. This in turn opened a way to measure the black hole mass by combining the radius from the time delay with the orbital velocity of the BLR clouds estimated from the emission line width and assuming the Kepler law for that purpose.

Numerous RM campaigns revealed a very strong and tight correlation between the BLR size and the monochromatic luminosity at 5100 Å (Peterson et al. 2004; Bentz et al. 2013). With this scaling, supermassive black hole mass measurements became possible, based just on a single spectrum (e.g. Vestergaard & Peterson 2006). This, in turn, opened a way for cosmological applications, since after proper calibration the time delay measurement allows to determine the luminosity, and to use a generalized standard candle approach to obtain the cosmological parameters (Watson et al. 2011; Haas et al. 2011; Czerny et al. 2013; King et al. 2014).

The problem has started with the detection of some outliers from the radius-luminosity relation. First, outliers have been found among the highly super-Eddington sources (Du et al. 2015, 2016, 2018), and their much shorter time delay than implied by the standard radius-luminosity relation (Bentz et al. 2013) could be interpreted as an effect of the self-shielding in the disk emission (Wang et al. 2014b).

Recently, shorter than expected time delays also were measured in some low Eddington ratio sources (Grier et al. 2017;

Du et al. 2018). It poses a question about the nature of the standard radius-luminosity relation and the physical reasons for the departures from this law. These shortened lags could be explained by retrograde accretion (Wang et al. 2014a; Du et al. 2018). Actually, the averaged radius of the BLR depends on the ionizing spectral energy distributions and spatial distributions of BLR clouds. The increase of scatterers around the canonical $R - L$ relation indicates a lack of understanding of the ionizing sources and the BLR itself.

Most of the models assume that the BLR is quasi-spherical, the radial extension of the cloud formation is not specified (e.g. Pancoast et al. 2014), and the clouds are exposed to the nuclear emission, so the BLR emissivity should respond to the bolometric luminosity of the nucleus or, more precisely, to the available ionizing continuum. This is why the ionization parameter U (see e.g. Wandel et al. 1999) was used in most of the past BLR modelling. Some models specified the inner BLR radius on some physical grounds (e.g. disk local self-gravity, Wang et al. 2011, 2012; dust presence in the accretion disk atmosphere, Czerny & Hryniewicz 2011; Czerny et al. 2015, 2017).

However, the relation between the 5100 Å monochromatic luminosity, L_{5100} , and the ionizing flux is non-linear and depends on the Spectral Energy Distribution (SED) of the source. Large black hole mass, low Eddington ratio and low spin lead to significant curvature of the spectrum in the UV band (e.g. Richards et al. 2006; Capellupo et al. 2015). In lower Eddington sources the inner disk may not be well represented by the standard accretion disk which effectively gives a similar result (see e.g. Kubota & Done 2018, and the references therein). Therefore, as argued by Wang et al. (2014a), we should expect significant dispersion if we use L_{5100} as a proxy for the ionizing flux, unless the spectrum shows no curvature due to a very high black hole spin in all sources. The need to return to the scaling with bolometric luminosity has been suggested by Trippe (2015). Kilerci Eser et al. (2015) showed observationally using seven well studied AGN that the relation between UV and optical flux is non-linear, and UV flux offers much better proxy for the ionizing flux and leads to the lower dispersion in the radius-luminosity relation.

In the present paper we adopt a general approach based on the assumption that the size of the BLR scales with the ionizing flux. However, as in Wang et al. (2014a), we take into account that the ionizing flux is not a linear function of the monochromatic luminosity. We consider the predictions for the ionizing flux from an accretion disk around a spinning black hole, together with the possibility of a counter-rotating disk and the possible existence of the inner hot flow instead of a standard optically thick cold accretion disk.

We consider the standard scenario of the BLR sensitive to the full ionizing flux available. In this model, the relation between the ionizing flux and the monochromatic luminosity at 5100 Å is not linear, and the size of the BLR is expected to depend on the black hole mass and the Eddington ratio. Additionally, there are two effects: (i) the spin of the black hole plays an important role, (ii) in the case of low Eddington ratio AGN the inner radius of the optically thick accretion disk might not be located at Innermost Stable Circular Orbit (ISCO) but further out, and in the innermost part the flow is replaced by optically thin and hot Advection Diminated Accretion Flow (ADAF). We consider these effects separately. The role of the spin as a possible source of dispersion and systematic departures from the simple radius-luminosity trend has already been studied by Wang et al. (2014a), but here we generalize the method and study the latter option of the inner ADAF.

2.1. Accretion disk model and ionizing flux

Since Wang et al. (2014a) showed that, most likely, a high value of spin is required, in the present paper we use the Novikov-Thorne model of the accretion disk (Novikov & Thorne 1973; Wang et al. 2014a). We combine the local emissivity with the ray tracing procedure applied earlier in Czerny et al. (2011) which allows us to include all relativistic corrections, including the light bending, gravitational redshift and Doppler boosting. The disk model is thus parametrized by the black hole mass, M_{\bullet} , accretion rate, \dot{M}_{\bullet} , and dimensionless spin parameter, a . We consider both prograde and retrograde spin values.

The calculation of the observed monochromatic luminosity in this model depends on the viewing angle, i , between the symmetry axis and the observer. We do not know this angle in individual sources, but the expected range of angles is constrained by the presence of the dusty-molecular torus (see Krolik 1999). The torus blocks the view toward the nucleus at high viewing angles, and such sources do not show their BLR, and they are classified as type 2 sources. Observational constraints on the torus opening angle are not simple, they typically imply a mean torus opening angle of order of 45° , and this value does not depend strongly on the source luminosity (e.g. Tovmassian 2001; Lawrence & Elvis 2010; He et al. 2018). Taking into account this constraint and assuming otherwise random orientation of AGN with respect to us we adopt the viewing angle $i \sim 30^{\circ}$ as a representative value. Thus we measure the observed fluxes assuming the same viewing angle for all the sources. We neglect here the effect of finite wavelength width for the hydrogen cross-section (see Eq. 5 of Wang et al. 2014a) and determine the luminosity at 13.6 eV (1 Rydberg) as

2. METHOD

$$L_{\text{ion}} = \nu L_{\nu}(1 \text{ Rydberg}) [\text{erg s}^{-1}]. \quad (1)$$

However, the BLR sees a different part of the spectrum. The BLR covers from 10% to 30% of the sky from the point of view of the inner disk, and it intercepts photons propagating relatively close to the equatorial plane (but not too close since highly inclined photons are intercepted by the disk itself). So, when calculating the number of ionizing photons we integrate the spectrum above 1 Ry over all viewing angles between 80° and 45°

$$Q = \int_{45^\circ}^{80^\circ} \int_{1 \text{ Rydberg}}^{\infty} \frac{L_\nu(\theta)}{h\nu} d\nu \sin \theta d\theta \text{ [photons s}^{-1}\text{]}. \quad (2)$$

The integration is performed far from the black hole, where the GR effects are already negligible. Photons propagating at angles larger than 80° are neglected since they will be absorbed by the disk itself. The ionization level of the BLR clouds can be estimated using either L_{ion} , or Q .

2.2. Accretion disks with inner ADAF

The transition from the outer cold disk to the inner hot disk is still debated, particularly for the galactic sources. However, it is clear that in very low luminosity sources (the most extreme case is Sgr A*) there is no cold outer disk. A series of papers discussed this issue on the basis of the radiative and conductive interaction between the hot corona above the disk and the underlying cold disk, and it was shown that for very low accretion rates the cold inner disk disappears (see Yuan & Narayan 2014, for a review). The inner flow then proceeds through an optically thin hot flow, such as ADAF (Ichimaru 1977; Narayan & Yi 1994) or its alternatives, e.g. Advection Dominated Inflow-Outflow Solutions (ADIOS; Blandford & Begelman 1999). Most of these solutions can be described under the common name RIAF (Radiatively Inefficient Accretion Flow) but some are actually quite radiatively efficient if the strong coupling exists between the hot ions and electrons (Bisnovatyi-Kogan & Lovelace 1997; Sironi & Narayan 2015). However, the common property of these solutions is that ion temperature is close to virial temperature, and electrons are also relatively hot so the emitted radiation concentrates in X-rays instead of far-UV local black body emission characteristic for the cold accretion disks.

For the purpose of this paper we use two prescriptions from Czerny et al. (2004). The first one is simply based on the *strong ADAF principle*, i.e. whenever the ADAF solution exists the flow proceeds through an ADAF-type flow, as in the classical papers (Abramowicz et al. 1995; Honma 1996; Kato & Nakamura 1998). The second option is based on evaporation of the cold disk caused by electron conduction between the disk and the two-temperature hot corona (Różańska & Czerny 2000a; Meyer & Meyer-Hofmeister 2002).

In the first case the transition from a cold disk to an ADAF flow occurs at

$$R_{\text{evap}} = 2.0 \alpha_{0.1}^4 \dot{m}^{-2} R_{\text{Schw}}, \quad (3)$$

(see e.g. Eq. 8 in Czerny et al. 2004), where \dot{m} is the dimensionless accretion rate, $\alpha_{0.1}$ is the viscosity parameter in units of 0.1, and R_{Schw} is the Schwarzschild radius of the black hole (equal $2 R_g = 2GM/c^2$). Here \dot{m} is defined for a fixed Newtonian efficiency of the accretion process

$$\dot{m} = \frac{\dot{M}_\bullet}{\dot{M}_{\text{Edd}}}; \quad \dot{M}_{\text{Edd}} = \frac{48\pi GM_\bullet m_p}{\sigma_T c}, \quad (4)$$

where m_p is the proton mass, and σ_T is the Thomson cross-section.

In the description of the second scenario we adopt Eq. 11 from Czerny et al. (2004) for the transition radius between the outer disk and an inner hot flow since it contains the effect of the magnetic pressure and compares most favourably with the observed extension of the BLR:

$$R_{\text{evap}} = 19.5 \alpha_{0.1}^{0.8} \beta^{-1.08} \dot{m}^{-0.53} R_{\text{Schw}}, \quad (5)$$

where β is the ratio of the total (gas + radiation) pressure to the total plus magnetic pressure and varies between 0 (magnetic pressure dominance) to 1 (no magnetic pressure). We neglect the emission from the inner hot flow because this very hot plasma, with electron temperature of the order of tens of keV, does not contribute to the 5100 \AA flux. This emission can to some extent affect the BLR by Compton-heating the clouds and the intercloud medium suppressing the line emission. However, since we are interested only in the ionization flux, and not in full radiative transfer computations with cooling/heating balance, we neglect this emission, effectively locating the inner disk radius at R_{evap} . In this scenario the dependence on the spin practically disappears since the outer disk is only weakly affected by the rotation of the central black hole.

2.3. BLR radius

We assume the standard view that the localization of the BLR is related to the ionizing flux. When we use L_{ion} defined in Eq. 1 we follow the approach of Wang et al. (2014a). We assume the scaling of R_{BLR} with the ionizing flux to have the form of a power law with the same index as determined by Bentz et al. (2013),

$$\log R_{\text{BLR}} = 0.542 \log L_{\text{ion}} + \text{const}, \quad (6)$$

where we specifically took the value of the index from their fit *Clean*. The value of constant has to be adjusted since now we use L_{ion} instead of L_{5100} as done in Bentz et al. (2013).

When we use Q as the parametrization of the incident flux, we follow even more classical approach to modelling of the

BLR. It was argued in the past that the BLR properties are well approximated by the fixed value of the ionization parameter, U , and the representative cloud density. The ionization parameter U is defined as

$$U = \frac{Q}{4\pi r^2 c n_e}, \quad (7)$$

(see e.g. [Ferland & Netzer 1983](#)) where n_e is the representative local density of the cloud, and Q is the number of ionizing photons (above 1 Rydberg) emitted by the accretion disk. We thus calculate the BLR radius from this formula,

$$\log R_{\text{BLR}} = 0.5 \log Q + \text{const.} \quad (8)$$

The value of the constant is then related to the universal values of U and n_e . The universal characteristic of the cloud density was argued for at the basis of the radiation pressure confinement mechanism ([Baskin & Laor 2018](#)).

2.4. Observational data

We compare the model with the size of the BLR measured as a delay with respect to H β line in reverberation campaigns. We use a compilation of the results available in the literature (see [Table 1](#)). The measurements come from various groups, most of them were performed for nearby sources. The sample of [Bentz et al. \(2013\)](#) has been carefully corrected for the contamination of the 5100 Å flux by the host galaxy. The sample from [Grier et al. \(2017\)](#) comes from SDSS-RM (Sloan Digital Sky Survey Reverberation Measurement) project and covers larger redshifts up to $z = 1.026$. The measurements by [Lu et al. \(2016\)](#) provide an independent determination of the delay in NGC 5548, and [Wang et al. \(2016\)](#) gives the delay measured for a gamma-ray loud NLS1. The sample from [Du et al. \(2014, 2015, 2016, 2018\)](#) papers represent SEAMBH (Super-Eddington Accretion in Massive Black Holes) project so on average these objects have higher Eddington ratios than sources from other samples. In diagrams we mark them with a different colour as they might bias the results. We also give in [Table 1](#) the black hole mass values taken from the references above, and the Eddington ratio which we calculate from that mass value and from the monochromatic luminosity assuming a fixed bolometric correction of 9.26 after [Shen et al. \(2011\)](#). Absolute values of the luminosity are given assuming the cosmological parameters: $H_0 = 67 \text{ km s}^{-1} \text{ Mpc}^{-1}$, $\Omega_\Lambda = 0.68$, $\Omega_m = 0.32$ ([Ade et al. 2014](#)).

3. RESULTS

We compare the measured time delays in monitored AGN with the model prediction of the position of the BLR radius taking into account two ways of connecting the BLR position with the incident radiation (through L_{ion} defined in [Eq. 1](#)

and Q defined in [Eq. 2](#)). The incident spectrum is calculated for a realistic range of black hole masses (from $10^6 M_\odot$ to $10^{10} M_\odot$) and Eddington luminosities (from 0.01 to 1.0). We allow for a broad range of spin, including the case of a counter-rotating black hole, and we also allow for the evaporation of the inner disk given by [Eq. 5](#).

Since the observational results are always plotted as a delay versus the monochromatic flux at 5100 Å but the ionization flux in general is not a linear function of that flux, we first show the representative examples of the incident spectra for the adopted parameter range (see [Fig. 1](#)). The relation between L_{ion} and the 5100 Å luminosity is almost linear when the Eddington ratio is large, the black hole mass is small, and the black hole spin large: in this regime the spectrum up to 912 Å is still well described by the canonical $\nu L_\nu \propto \nu^{4/3}$ law. Outside this regime, the maximum temperature of the accretion disk drops, and the SED peak moves into UV band, leading to a strong spectral curvature. A similar effect would be caused by the inner disk evaporation but the presented examples illustrate accretion disks extending down to Innermost Stable Circular Orbit (ISCO). The disk spectral curvature leads to a slower rise of L_{ion} in comparison to L_{5100} in a sequence of models with a constant Eddington rate and rising black hole mass. We take into account this effect in interpreting the data, since we calculate the expected time delay from L_{ion} (or Q).

We now calculate the expected time delays from our grid of models at the basis of the ionized flux, but we show the resulting delays as a function of the monochromatic flux since the observational results are customarily presented in this way. We compare the predicted delay grid with the measurements of the H β delays given in [Table 1](#).

3.1. BLR size from the ionizing luminosity

Since our sample is larger than the sample considered in [Wang et al. \(2014a\)](#), we first use the same method as was used there, with BLR distance measured from ionizing flux L_{ion} estimated at 912 Å (see [Eq. 1](#)), and without any evaporation effect. The results are shown in [Fig. 2](#).

We see that the change of the sample essentially affects the conclusion reached by [Wang et al. \(2014a\)](#). Their conclusion was that all the monitored objects must have predominantly high spin since at that time most of the measured delays were located along the $\tau \propto L_{5100}^{1/2}$ line. Currently, with the presence of many shorter lags in the sample, good coverage of the measured distribution of the time delays is achieved if we allow a whole range of black hole spins from 0 to maximally rotating black holes. A few objects require counter-rotating spin. What is interesting, however, these objects have rather moderate luminosities, $\sim 10^{44} \text{ erg s}^{-1}$, relatively low Eddington ratios, ~ 0.05 , and black hole masses which are also moderate, $\sim 10^8 - 10^9 M_\odot$. These values are roughly con-

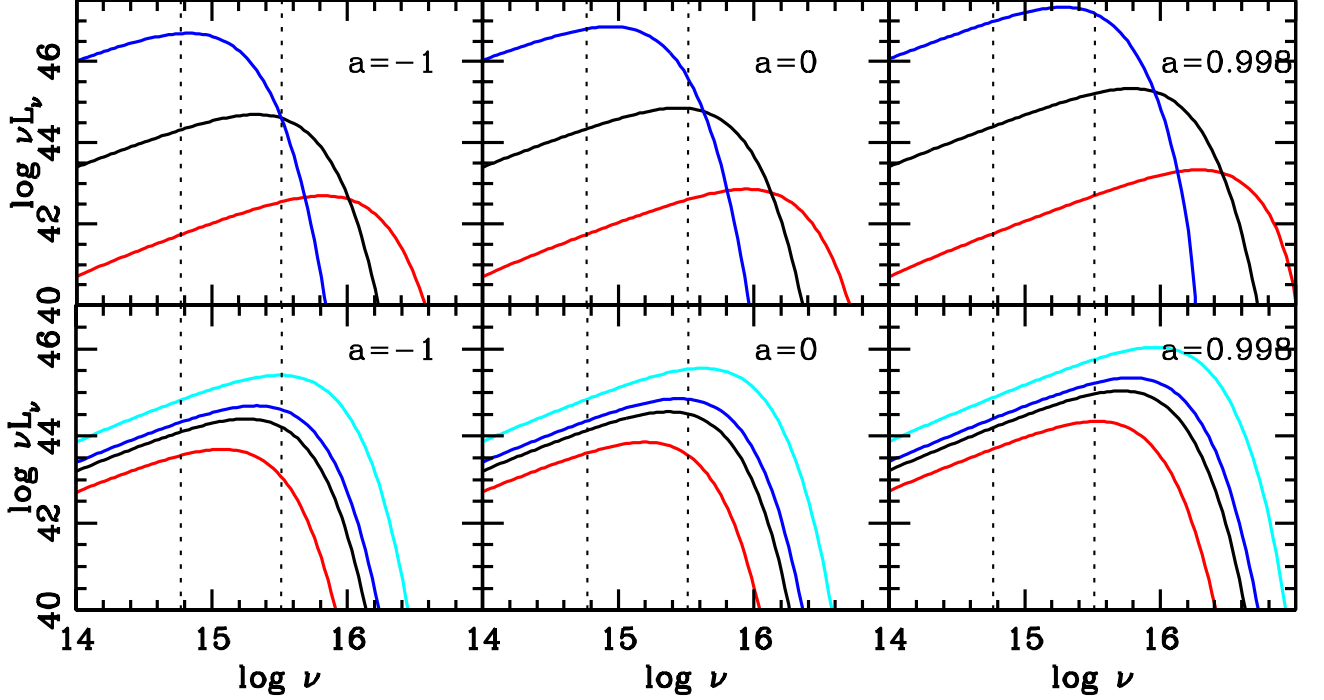


Figure 1. The examples of the accretion disk spectra for the parameter range covered by our computations. Upper panels shows spectra for a fixed Eddington ratio 0.1, and black hole masses $10^6 M_\odot$ (red), $10^8 M_\odot$ (black), and $10^{10} M_\odot$ (blue lines), lower panel shows spectra for a black hole mass $10^8 M_\odot$ and eddington ratio 0.01 (red), 0.05 (black), 0.1 (blue), and 0.5 (cyan). The three columns represent three spin values. Dotted lines indicate the position of the usual continuum measurement at 5100 \AA , and the Lyman edge where ionizing flux should be evaluated.

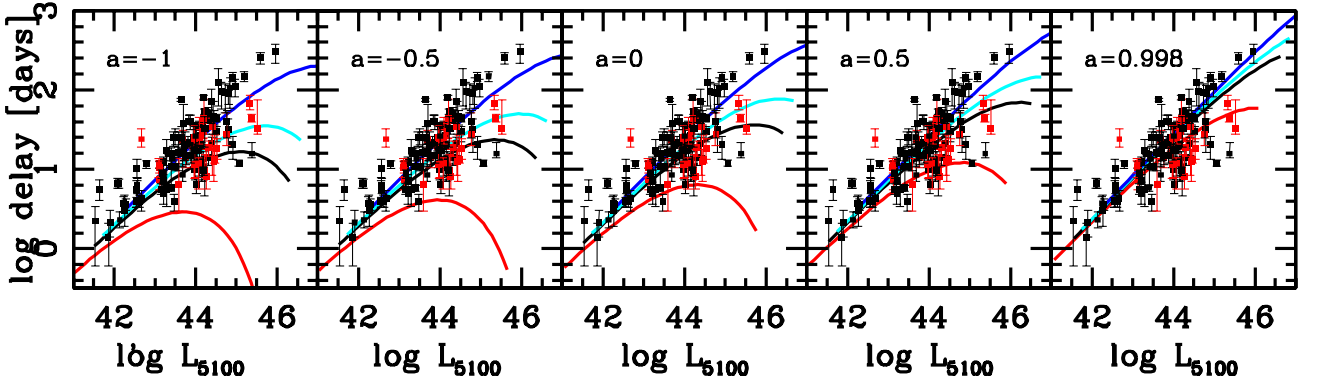


Figure 2. The dependence of the size of the BLR, expressed in terms of the time delay, calculated from L_{ion} for a range of spin (separate panels), and Eddington ratio $\dot{m} = 0.01$ (red line), $\dot{m} = 0.05$ (black line), $\dot{m} = 0.1$ (cyan line), and $\dot{m} = 0.5$ (blue line) as a function of monochromatic luminosity at 5100 \AA . Observational points come from Table 1, super-Eddington sources are marked in red.

sistent with the parameters of the sources in the SDSS-RM sample of Grier et al. (2017). Such accretion rates are relatively low for a quasar sample but this is the consequence of the selection effect: the monitoring was short, about a year, so the delays were measured only for the sources with delays shorter than 100 days in the observed frame, so only for the low luminosity tail of the sample. The model predicts even shorter time delays than measured for more massive sources but observationally determined delays do not populate this region. This is because we allowed for even lower Eddington

ratios (0.01) and larger masses ($10^{10} M_\odot$) in our parameter grid than present in the sample.

3.2. BLR size from the number of ionizing photons

Next we use the R_{BLR} predictions based on the number of photons Q intercepted by the BLR (see Eq. 2), again without any evaporation effect, and the results are shown in Fig. 3. The model predictions are qualitatively similar, but not identical. Overall, Q prescription gives much stronger bending effect for a counter-rotating accretion disk than the model based on L_{ion} for the same parameters. The trend reverses

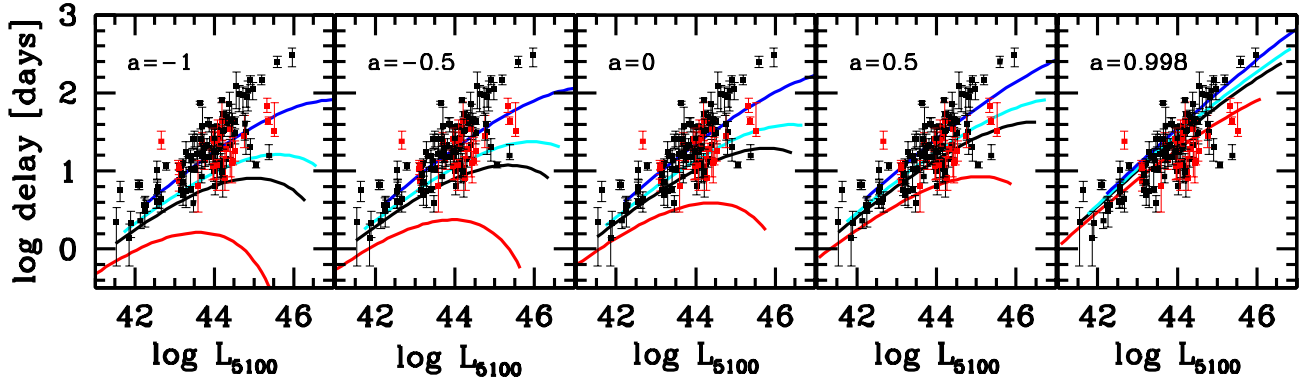


Figure 3. The same as Fig. 2 but for the size of the BLR calculated from Q .

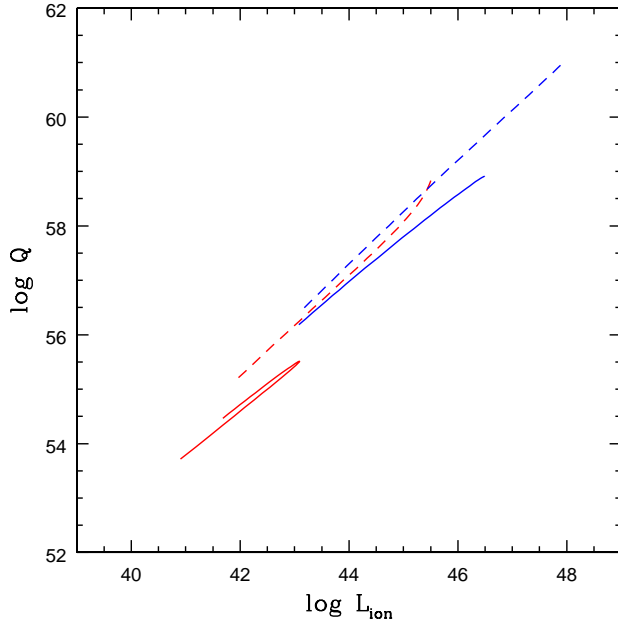


Figure 4. The relation between the ionization luminosity L_{ion} and the number of ionizing photons, Q , for the size of the BLR for $a = -1.0$ (dashed lines), and $a = 0.998$ (continuous lines), for two values of the accretion rate $\dot{m} = 0.01$ (red lines), and $\dot{m} = 0.5$ (blue lines). Both L_{ion} and Q are not monotonic functions of the black hole mass, as reflected on turn-over loop, but the two quantities are not strictly proportional to each other.

for high spin co-rotating accretion disk, when smaller departure from a power law trend is seen for Q -based model. This is related to the relativistic effects. For large black hole spin in a corotating disk the radiation emitted at higher inclination angles is strongly beamed and enhanced in comparison with the continuum measured by an observer, which compensates for the spectral bending seen in Fig. 1. This also means that Q is not strictly proportional to L_{ion} . We illustrate this effect in Fig. 4. The departure from the strict linearity between the two quantities results both from the derivation of Q as an integral, and from the relativistic effects (a difference between photons going to observer and photons going toward BLR). The approach based on Q is more accurate, and the examples

calculated later on are based on this assumption but overall the difference between L_{ion} and Q predictions is not large and L_{ion} approach is equally useful for statistical analysis of the samples.

Now we compare Q -based delay predictions to the measured time delays (see Fig. 3). This approach does not require counter-rotating black holes to explain even the shortest time lags. Therefore, with very simple and basic assumptions (standard Novikov-Thorne disk, co-rotating with a black hole, with a range of masses, accretion rates and spins, BLR responding to the ionizing continuum at fixed ionization parameter and density) we are able to reproduce fully satisfactorily the observed distribution of the time delays.

However, the assumption that the cold Keplerian disk extends all the way down to ISCO is under discussion, particularly for lower Eddington ratio sources. If the inner hot flow develops, this part of the disk is not longer a source of UV photons but instead, filled with a hot plasma at electron temperatures of order of 100 keV is a source of X-ray emission. Effectively this decreases the number of photons available for ionizing hydrogen. Available models allow to determine the position of this transition and thus are subject of tests if the predictions are consistent with the observed time delays.

3.3. BLR size with inner hot flow in classical ADAF scenario

We first test the prediction of the model based on *strong ADAF principle* described by Eq. 3. For the viscosity parameter, we assume the value $\alpha = 0.02$ which was suggested by direct studies of the quasar UV variability (Siemiginowska & Czerny 1989; Starling et al. 2004), and is consistent with Damped Random Walk results (Kelly et al. 2009; see also the discussion in Grzędzielski et al. 2017). The results are shown in Fig. 5. In this case no counter-rotating spin values are necessary, and the whole plane is well covered even if all the objects have high spin (left panel). The longest delays for a given value of L_{5100} require high spin values while shorter delays may imply either lower spin or lower Eddington ratio. This degeneracy can be removed if we actually have reliable

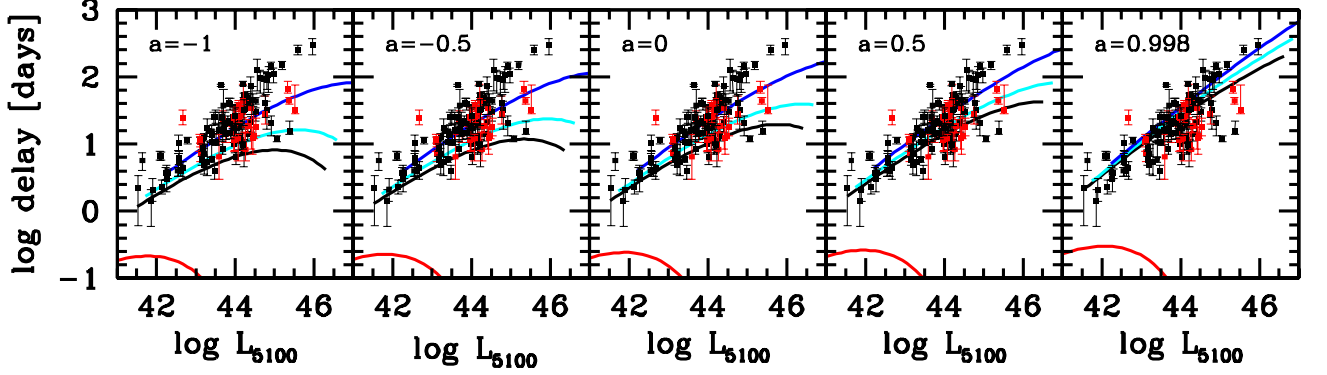


Figure 5. The dependence of the size of the BLR calculated from Q when ADAF principle is assumed, for a range of spins (separate panels), and Eddington ratios $\dot{m} = 0.01$ (red line), $\dot{m} = 0.05$ (black line), $\dot{m} = 0.1$ (cyan line), and $\dot{m} = 0.5$ (blue line) as a function of monochromatic luminosity at 5100 Å. Model parameter: $\alpha = 0.02$. Observational points come from Table 1, super-Eddington sources are marked in red.

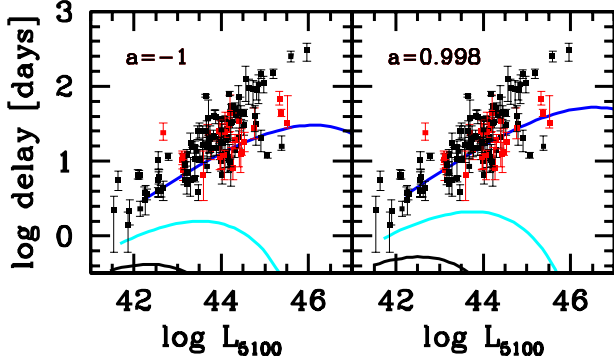


Figure 6. The dependence of the size of the BLR calculated from Q when evaporation of the inner disk is included, for a maximally counter-rotating spin (left panel, ISCO radius $9 R_g$), and maximally co-rotating spin (right panel, ISCO radius $1.24 R_g$), and Eddington ratios $\dot{m} = 0.01$ (red line), $\dot{m} = 0.05$ (black line), $\dot{m} = 0.1$ (cyan line), and $\dot{m} = 0.5$ (blue line) as a function of monochromatic luminosity at 5100 Å. Evaporation model parameters: $\alpha = 0.02$, $\beta = 0.5$. Observational points come from Table 1, super-Eddington sources are marked in red.

determination of the Eddington ratio for an individual object. However, in comparison with the predictions for the disk without an inner cut-off the requested accretion rates of sources with short delays are much higher, all observed sources are then predicted to have Eddington ratios above ~ 0.05 . Some of the Eddington ratios in the SDSS-RM sample may be lower than this limit if the bolometric luminosity is estimated as roughly 9 times the L_{5100} luminosity and the black hole mass measurement from Grier et al. (2017) is adopted. On the other hand, such an estimate of the bolometric luminosity is highly uncertain since it does not take into account the differences in the spectral shapes clearly seen in Fig. 1.

3.4. BLR size with inner hot flow defined by inner disk evaporation

Finally, we test the solutions based on the evaporation of the inner disk as described by Eq. 5. The results obtained for

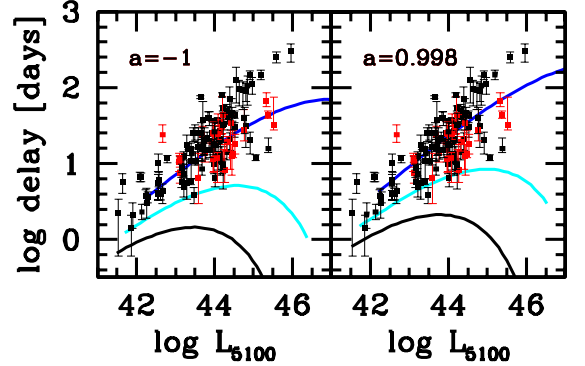


Figure 7. The same as Fig. 6 but for the magnetization parameter $\beta = 0.99$.

the parameters $\alpha = 0.02$ and $\beta = 0.5$ (moderate magnetic field strength; see Eq. 5) are far from being satisfactory (see Fig. 6). The longest time delays are not reproduced, even if we allow for high spin since the transition radius between the outer cold disk and an inner hot flow is far too large. Significant contribution of the magnetic field to the total pressure in the disk is inconsistent with the observational data. We thus decreased the role of the magnetic field, assuming $\beta = 0.99$ (i.e. only 1 % of the contribution from the magnetic pressure to the gas plus radiation pressure) but such parameter adjustment still did not fully solve the problem (see Fig. 7). We thus additionally allowed for a significant decrease of the viscosity parameter down to the value $\alpha = 0.001$. For these parameters, evaporation of the outer cold disk is indeed inefficient. The transition radius between the outer cold disk and an inner hot flow takes place at $5.7 R_{\text{Schw}}$ for the Eddington ratio 0.01 and it is closer in or absent for larger accretion rates and/or lower spin. When we assumed the expected values of the viscosity parameter $\alpha = 0.02$, the transition radii start at $62.3 R_{\text{Schw}}$ (for the lowest Eddington ratio 0.01). This low viscosity $\alpha \sim 0.001$ is thus strongly required if the measured time delays are to be consistent with the disk evaporation phenomenon.

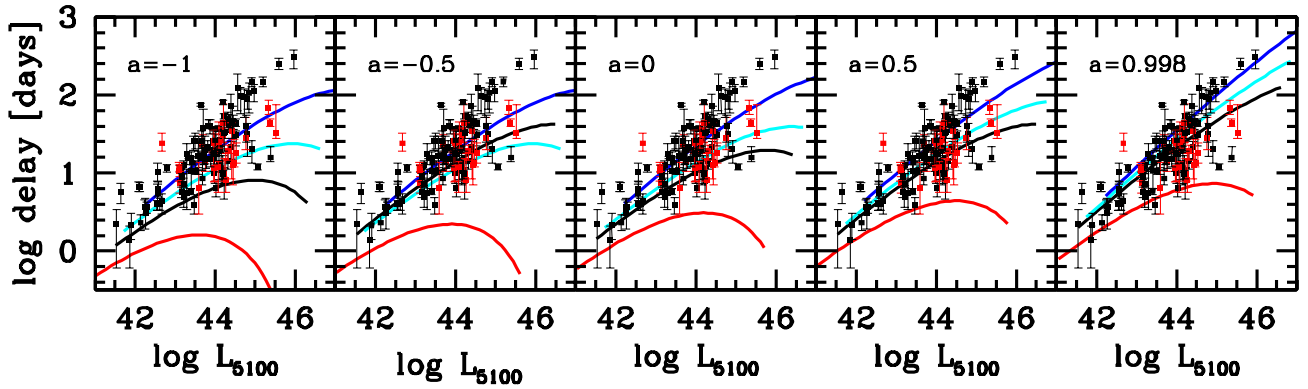


Figure 8. The dependence of the size of the BLR calculated from Q when evaporation of the inner disk is included, for a range of spin (separate panels), and Eddington ratio $\dot{m} = 0.01$ (red line), $\dot{m} = 0.05$ (black line), $\dot{m} = 0.1$ (cyan line), and $\dot{m} = 0.5$ (blue line) as a function of monochromatic luminosity at 5100 Å. Evaporation model parameters: $\alpha = 0.001$, $\beta = 0.99$. Observational points come from Table 1, super-Eddington sources are marked in red.

However, as we mentioned before, such small values of the viscosity parameter are not supported by the quasar variability (see Grzędzielski et al. 2017). This implies that the physically-based description of the disk evaporation and the transition to inner hot flow still requires a more advanced approach. The issue is difficult, and subject of studies since several years in the context of cataclysmic variables (Meyer & Meyer-Hofmeister 1994), binary black holes and AGN (Liu et al. 1999; Różańska & Czerny 2000b). The transition process is further complicated by the possibility of the existence of the inner cool disk separated by the gap of pure hot flow from the outer cold disk (Liu et al. 2006; Meyer et al. 2007; see Meyer-Hofmeister & Meyer 2014; Meyer-Hofmeister et al. 2017; Taam et al. 2018 for recent developments). Here we considered only the inner radius of the outer cold disk.

4. DISCUSSION

4.1. The BLR models

Emission lines of the BLR respond to the emission originating close to the black hole, as clearly seen from the response of the line with respect to the variable incident flux. Traditionally, this response was modeled by parametrizing the incident continuum with a single parameter in the form of the ionization parameter, or ionizing flux. Then, if a range of radii and densities were allowed, like for example in the LOC model (Baldwin et al. 1995) line ratios were successfully modelled. However, this general approach did not give a direct insight into the reason for the presence of the numerous clouds above the disk. Wind models are also parametric and not quite constraining the cloud formation mechanisms. The observational discovery of the scaling of the BLR size with a monochromatic flux instead of the ionizing flux opened a way for testing the cloud origin. Such a scaling, with a very small dispersion, is consistent with the dust-based formation mechanism of the BLR (Czerny & Hryniewicz 2011; Czerny

et al. 2015, 2017; Baskin & Laor 2018), at least with respect to the $H\beta$ formation region. In this model the BLR position is controlled not by the ionizing flux but by the availability of the material for the irradiation, lifted above the disk by the dust-driven radiation pressure. This scaling also strongly disfavoured self-gravitational instability as the BLR origin (Czerny et al. 2016).

New observational data presented in Fig. 2 drastically changes this view. Now the dispersion around the delay-monochromatic flux relation is very large, and most of the new measurements lie below the previous tight scaling law of Bentz et al. (2013). Part of the outliers come from the super-Eddington ratio sample by Du et al. (2014, 2015, 2016, 2018), and in this case the departure from the previous scaling can be explained as a departure from the thin Keplerian disk approximation for the incident continuum. The average value of the Eddington ratio in these sources is 1.72. However, other numerous points come from the SDSS-RM sample of Grier et al. (2017), and these objects have low to moderate Eddington ratios, with the average value of 0.24, not significantly higher than in the Bentz et al. (2013) sample (0.14), well within the dispersion in the two samples.

The measurements we use here come from the literature, as described in Sect. 2.4, and were not prepared in a uniform way. All sources in Bentz et al. (2013) sample were carefully corrected for the host galaxy contamination using Hubble Space Telescope (HST) observations, and the corrections were important not just for the faintest nearby AGN but also for PG quasars (Bentz et al. 2006). Good example from Bentz et al. (2013) is the source SBS 116+583A ($z = 0.02787$) where the AGN emission contributes only 12% to the total flux at 5100 Å, i.e. not correcting this source for starlight gives a shift of 0.92 in the logarithm of L_{5100} , or, equivalently, a factor 2.9 in the expected time delay. The sources from Du et al. (2014) were also corrected for the starlight using HST images, while for the sources reported

later (Du et al. 2015, 2016, 2018) the authors used an empirical relation from Shen et al. (2011). Grier et al. (2017) used the information on host contamination from Shen et al. (2015) who has employed Principal Component Analysis (PCA) and the measurements of the measured stellar velocity dispersion to decompose the spectra into AGN and host components. The accuracy of such methods is difficult to estimate. The error in the host subtraction can be responsible for the incorrect determination of L_{5100} .

New results, if reliable, take us all the way back to the original concept of the simple BLR response to the ionizing flux. The range of delays are well consistent with the predictions of the ionized continuum based on the thin Keplerian disk since this ionized continuum does not scale linearly with the monochromatic flux at 5100 Å due to the curvature of the spectrum in the UV band (see Fig. 1). Models based on the dusty origin of the BLR seem not justified, as in this case no departure from Bentz et al. (2013) scaling is predicted for a broad range of black hole mass and accretion rates. Instead, the observed delays are consistent with a universal ionization parameter, and universal density in the H β formation region for a very broad range of parameters.

The range of spin plays an important role, and all spins from non-rotating black holes to maximally spinning ones ($a = 0.998$) are requested to create the appropriate representation of the reverberation studies sources. Counter-rotating disks are not strongly required but a small fraction of such sources is not excluded. Evaporation of the inner disk and a transition to ADAF are not really required for Eddington ratios above 1% studied here, and models which predict inner ADAF flow at such high Eddington ratios are disfavoured, so the models with an inner cold disk separated from the other cold disk sound more attractive. However, the predictions for such models are more complex and were not tested in detail in the current paper. In this paper we also did not test again the self-gravity scenario, but since self-gravity in general predicts shorter delays than Bentz et al. (2013) relation it remains to check if this option offers equally good coverage of the parameter space as a simple universal ionization parameter with universal density model.

Recently, a new model of the BLR origin was suggested by Wang et al. (2017). In this model, clumps in dusty/molecular torus are tidally captured and disrupted by the central black hole. A population of inflowing clouds forms at the first stage, a tiny fraction of clumps is channelled into outflows (less than 10%), and then most of the disrupted clumps form a BLR disk with Keplerian rotation (virialized component). Unlike the dust-based clouds (Czerny & Hryniewicz 2011), the supply of the BLR clouds originates from the dusty torus. The virialized component in this model can produce the canonical $R - L$ relation for sub-Eddington AGNs provided the ionisation parameter, density and temperature are univer-

sal. Additionally, the infalling component is supported by PG 2130+099 (see Sect. 4.3). This model avoids difficulties of disk self-gravity model or dust-based failed winds.

4.2. Implications to BH evolution

What we found in this paper is the role of black hole spin in the observed $R - L$ relation jointly with accretion rates. The vindication in support of retrograde accretion onto black holes has very important implications for cosmological evolution of black holes. If the black holes are fuelled in a stochastic manner, with no preferred orientation, they are slowly spinning due to cancellation of random angular momentum of accreted gas (King et al. 2008). Wang et al. (2009) built up an equation of the radiative efficiency (η) across cosmic time from observed data of galaxy and quasar surveys. The authors derived the evolutionary curve and obtained that the radiative efficiency changes from $\eta \approx 0.3$ at redshift $z \approx 2$, where quasar density peaks, down to 0.03 at low redshift. This supports the role of episodic accretion at later stages of the galaxy evolution. The downsizing behaviour of spins was further discussed by Li et al. (2012). Subsequently, Volonteri et al. (2013) found a similar behaviours of spin evolution from numerical simulations. The sensitive dependence of the $R - L$ relation on spin offers a new tool of estimating black hole rotation, in particular for those AGN with the retrograde accretion disks which may have too weak gravitational effects on iron K α line profiles to measure their spins from X-ray observations.

4.3. Future RM-campaigns

To draw firm conclusions, however, the measured delays have to be accurate. SDSS-RM campaign concentrated on average on higher redshift sources, the campaign was relatively short, and the observational cadence was not very dense. Determination of the time delays in AGN is not very straightforward since the variability has a red noise character, and the resprocessing region is extended. Frequently, two peaks show up in the cross correlation function (e.g. Du et al. 2016), and if the campaign is too short only one solution (the shorter one) may be found although it may not be actually the correct one. Therefore, an extension of this campaign is clearly necessary to ensure that the measured delays are not affected by the way how they are performed.

The cadence selected for RM-campaign is very important. Low-cadence campaign will smear short timescale variations so that the measured lags tend to be longer. PG 2130+099 is an example. Kaspi et al. (2000) measured a H β line lag of 188 days with a low cadence of about ~ 20 days and a couple of seasonal gaps, with the total campaign duration as long as about 8 years. With a cadence of a few days, however, Grier et al. (2008) measured a lag of ~ 23 days with large uncertainties (but the total length in their case was

only about 100 days). Moreover, Grier et al. (2012) got a lag of ~ 10 days with one day cadence. Hu et al. (2018) (ApJ, submitted) measured a lag of ~ 24 days with a cadence of 3 days, confirming the results of Grier et al. (2008), but found that the lag of ~ 188 days follows the dust reverberation scaling relation (Koshida et al. 2014), suggesting that the reverberations with a lag of 188 days are from the inner edge of the torus. This supports the ideas of Wang et al. (2017). Additionally, PG 2130+099 is a super-Eddington source and the other two lags of ~ 10 and ~ 24 days can be explained by the self-shadowing effects of slim accretion disks (Wang et al. 2014b). Overall, the BLR is extended, and the choice of the cadence can focus the monitoring on a particular part of the BLR, making a comparison of results for different sources very difficult. Also non-linear response of the BLR to the line emission, particularly if the characteristic variability timescale is short in comparison to the average time delay can easily lead to apparent shortening of the time delay, as pointed out by Goad & Korista (2014). Future RM-campaigns should be planned very carefully with respect to the cadence.

5. CONCLUSIONS

In this paper, we have tested roles of the energy distribution of accretion disks governed by black hole spins and accretion rates to the $R - L$ relation. Our main conclusions can be summarized in several points:

- New measurements of the time delays in AGN, inconsistent with the simple scaling relationship of Bentz et al. (2013) with the monochromatic flux, favor a model where the BLR responds to the ionizing continuum, and both the local density and the ionization parameter are universal, independent from the black hole mass and Eddington ratio. Inconsistency between

the results in Grier et al. (2017) and Bentz et al. (2013) does not seem to be related to the Eddington ratio, only slightly higher in the Grier et al. sample.

- Since new BLR scaling is sensitive to the SED shape, the radius-luminosity relation is a potential tool to examine the SED from an accretion disk.
- If the transition to the inner hot flow is based on *strong ADAF principle* the measured delays are consistent with the model for a realistic value of the viscosity parameter α because it does not overestimate the cold disk evaporation.
- If the transition to the inner hot flow is based on the disk evaporation through the electron conduction between the disk and the corona, low values of the magnetic pressure and very low values of the viscosity parameter α are required, so this description is less satisfactory than simple *strong ADAF principle*, and most likely implies that the inner cold disk formation takes place.
- New measurements can be seen as a counter-argument against the dust-based model of the BLR formation since dust-based model implies a scaling of the BLR size with the monochromatic flux.
- A confirmation of the new reverberation measurements for the outliers from the Bentz et al. (2013) relationship at low/moderate Eddington ratios is strongly required.

ACKNOWLEDGEMENTS

The project was partially supported by National Science Centre, Poland, grant No. 2017/26/A/ST9/00756 (Maestro 9). VK acknowledges Czech Science Foundation No. 17-16287S.

REFERENCES

- Abramowicz, M. A., Chen, X., Kato, S., Lasota, J.-P., & Regev, O. 1995, ApJL, 438, L37, doi: [10.1086/187709](https://doi.org/10.1086/187709)
- Ade, P., Aghanim, N., Armitage-Caplan, C., & et al. 2014, A&A, 571, A16, doi: [10.1051/0004-6361/201321591](https://doi.org/10.1051/0004-6361/201321591)
- Baldwin, J., Ferland, G., Korista, K., & Verner, D. 1995, ApJL, 455, L119, doi: [10.1086/309827](https://doi.org/10.1086/309827)
- Baskin, A., & Laor, A. 2018, MNRAS, 474, 1970, doi: [10.1093/mnras/stx2850](https://doi.org/10.1093/mnras/stx2850)
- Bentz, M. C., Peterson, B. M., Pogge, R. W., Vestergaard, M., & Onken, C. A. 2006, ApJ, 644, 133, doi: [10.1086/503537](https://doi.org/10.1086/503537)
- Bentz, M. C., Denney, K. D., Grier, C. J., et al. 2013, ApJ, 767, 149, doi: [10.1088/0004-637X/767/2/149](https://doi.org/10.1088/0004-637X/767/2/149)
- Bisnovatyi-Kogan, G. S., & Lovelace, R. V. E. 1997, ApJL, 486, L43, doi: [10.1086/310826](https://doi.org/10.1086/310826)
- Blandford, R. D., & Begelman, M. C. 1999, MNRAS, 303, L1, doi: [10.1046/j.1365-8711.1999.02358.x](https://doi.org/10.1046/j.1365-8711.1999.02358.x)
- Capellupo, D. M., Netzer, H., Lira, P., Trakhtenbrot, B., & Mejía-Restrepo, J. 2015, MNRAS, 446, 3427, doi: [10.1093/mnras/stu2266](https://doi.org/10.1093/mnras/stu2266)
- Czerny, B., Du, P., Wang, J.-M., & Karas, V. 2016, ApJ, 832, 15, doi: [10.3847/0004-637X/832/1/15](https://doi.org/10.3847/0004-637X/832/1/15)
- Czerny, B., & Hryniewicz, K. 2011, A&A, 525, L8, doi: [10.1051/0004-6361/201016025](https://doi.org/10.1051/0004-6361/201016025)
- Czerny, B., Hryniewicz, K., Maity, I., et al. 2013, A&A, 556, A97, doi: [10.1051/0004-6361/201220832](https://doi.org/10.1051/0004-6361/201220832)

- Czerny, B., Hryniewicz, K., Nikolajuk, M., & Sądowski, A. 2011, *MNRAS*, 415, 2942, doi: [10.1111/j.1365-2966.2011.18912.x](https://doi.org/10.1111/j.1365-2966.2011.18912.x)
- Czerny, B., Różańska, A., & Kuraszek, J. 2004, *A&A*, 428, 39, doi: [10.1051/0004-6361:20040487](https://doi.org/10.1051/0004-6361:20040487)
- Czerny, B., Modzelewska, J., Petrogalli, F., et al. 2015, *Advances in Space Research*, 55, 1806, doi: [10.1016/j.asr.2015.01.004](https://doi.org/10.1016/j.asr.2015.01.004)
- Czerny, B., Li, Y.-R., Hryniewicz, K., et al. 2017, *ApJ*, 846, 154, doi: [10.3847/1538-4357/aa8810](https://doi.org/10.3847/1538-4357/aa8810)
- Du, P., Hu, C., Lu, K.-X., et al. 2014, *ApJ*, 782, 45, doi: [10.1088/0004-637X/782/1/45](https://doi.org/10.1088/0004-637X/782/1/45)
- . 2015, *ApJ*, 806, 22, doi: [10.1088/0004-637X/806/1/22](https://doi.org/10.1088/0004-637X/806/1/22)
- Du, P., Lu, K.-X., Zhang, Z.-X., et al. 2016, *ApJ*, 825, 126, doi: [10.3847/0004-637X/825/2/126](https://doi.org/10.3847/0004-637X/825/2/126)
- Du, P., Zhang, Z.-X., Wang, K., et al. 2018, *ApJ*, 856, 6, doi: [10.3847/1538-4357/aaae6b](https://doi.org/10.3847/1538-4357/aaae6b)
- Ferland, G. J., & Netzer, H. 1983, *ApJ*, 264, 105, doi: [10.1086/160577](https://doi.org/10.1086/160577)
- Goad, M. R., & Korista, K. T. 2014, *MNRAS*, 444, 43, doi: [10.1093/mnras/stu1456](https://doi.org/10.1093/mnras/stu1456)
- Grier, C. J., Peterson, B. M., Bentz, M. C., et al. 2008, *ApJ*, 688, 837, doi: [10.1086/592269](https://doi.org/10.1086/592269)
- Grier, C. J., Peterson, B. M., Pogge, R. W., et al. 2012, *ApJ*, 755, 60, doi: [10.1088/0004-637X/755/1/60](https://doi.org/10.1088/0004-637X/755/1/60)
- Grier, C. J., Trump, J. R., Shen, Y., et al. 2017, *ApJ*, 851, 21, doi: [10.3847/1538-4357/aa98dc](https://doi.org/10.3847/1538-4357/aa98dc)
- Grzędziński, M., Janiuk, A., Czerny, B., & Wu, Q. 2017, *A&A*, 603, A110, doi: [10.1051/0004-6361/201629672](https://doi.org/10.1051/0004-6361/201629672)
- Haas, M., Chini, R., Ramolla, M., et al. 2011, *A&A*, 535, A73, doi: [10.1051/0004-6361/201117325](https://doi.org/10.1051/0004-6361/201117325)
- He, Z., Sun, A.-L., Zakamska, N. L., et al. 2018, *MNRAS*, 478, 3614, doi: [10.1093/mnras/sty1322](https://doi.org/10.1093/mnras/sty1322)
- Honma, F. 1996, *PASJ*, 48, 77, doi: [10.1093/pasj/48.1.77](https://doi.org/10.1093/pasj/48.1.77)
- Ichimaru, S. 1977, *ApJ*, 214, 840, doi: [10.1086/155314](https://doi.org/10.1086/155314)
- Kaspi, S., Smith, P. S., Netzer, H., et al. 2000, *ApJ*, 533, 631, doi: [10.1086/308704](https://doi.org/10.1086/308704)
- Kato, S., & Nakamura, K. E. 1998, *PASJ*, 50, 559, doi: [10.1093/pasj/50.6.559](https://doi.org/10.1093/pasj/50.6.559)
- Kelly, B. C., Bechtold, J., & Siemiginowska, A. 2009, *ApJ*, 698, 895, doi: [10.1088/0004-637X/698/1/895](https://doi.org/10.1088/0004-637X/698/1/895)
- Kilerci Eser, E., Vestergaard, M., Peterson, B. M., Denney, K. D., & Bentz, M. C. 2015, *ApJ*, 801, 8, doi: [10.1088/0004-637X/801/1/8](https://doi.org/10.1088/0004-637X/801/1/8)
- King, A. L., Davis, T. M., Denney, K. D., Vestergaard, M., & Watson, D. 2014, *MNRAS*, 441, 3454, doi: [10.1093/mnras/stu793](https://doi.org/10.1093/mnras/stu793)
- King, A. R., Pringle, J. E., & Hofmann, J. A. 2008, *MNRAS*, 385, 1621, doi: [10.1111/j.1365-2966.2008.12943.x](https://doi.org/10.1111/j.1365-2966.2008.12943.x)
- Koshida, S., Minezaki, T., Yoshii, Y., et al. 2014, *ApJ*, 788, 159, doi: [10.1088/0004-637X/788/2/159](https://doi.org/10.1088/0004-637X/788/2/159)
- Krolik, J. H. 1999, *Active galactic nuclei : from the central black hole to the galactic environment*
- Kubota, A., & Done, C. 2018, *ArXiv e-prints*, <https://arxiv.org/abs/1804.00171>
- Lawrence, A., & Elvis, M. 2010, *ApJ*, 714, 561, doi: [10.1088/0004-637X/714/1/561](https://doi.org/10.1088/0004-637X/714/1/561)
- Li, Y.-R., Wang, J.-M., & Ho, L. C. 2012, *ApJ*, 749, 187, doi: [10.1088/0004-637X/749/2/187](https://doi.org/10.1088/0004-637X/749/2/187)
- Liu, B. F., Meyer, F., & Meyer-Hofmeister, E. 2006, *A&A*, 454, L9, doi: [10.1051/0004-6361:20065430](https://doi.org/10.1051/0004-6361:20065430)
- Liu, B. F., Yuan, W., Meyer, F., Meyer-Hofmeister, E., & Xie, G. Z. 1999, *ApJL*, 527, L17, doi: [10.1086/312383](https://doi.org/10.1086/312383)
- Liutiy, V. M. 1977, *Soviet Ast.*, 21, 655
- Lu, K.-X., Du, P., Hu, C., et al. 2016, *ApJ*, 827, 118, doi: [10.3847/0004-637X/827/2/118](https://doi.org/10.3847/0004-637X/827/2/118)
- Meyer, F., Liu, B. F., & Meyer-Hofmeister, E. 2007, *A&A*, 463, 1, doi: [10.1051/0004-6361:20066203](https://doi.org/10.1051/0004-6361:20066203)
- Meyer, F., & Meyer-Hofmeister, E. 1994, *A&A*, 288, 175
- . 2002, *A&A*, 392, L5, doi: [10.1051/0004-6361:20021075](https://doi.org/10.1051/0004-6361:20021075)
- Meyer-Hofmeister, E., Liu, B. F., & Qiao, E. 2017, *A&A*, 607, A94, doi: [10.1051/0004-6361/201731105](https://doi.org/10.1051/0004-6361/201731105)
- Meyer-Hofmeister, E., & Meyer, F. 2014, *A&A*, 562, A142, doi: [10.1051/0004-6361/201322423](https://doi.org/10.1051/0004-6361/201322423)
- Narayan, R., & Yi, I. 1994, *ApJL*, 428, L13, doi: [10.1086/187381](https://doi.org/10.1086/187381)
- Novikov, I. D., & Thorne, K. S. 1973, in *Black Holes (Les Astres Occlus)*, ed. C. Dewitt & B. S. Dewitt, 343–450
- Pancoast, A., Brewer, B. J., Treu, T., et al. 2014, *MNRAS*, 445, 3073, doi: [10.1093/mnras/stu1419](https://doi.org/10.1093/mnras/stu1419)
- Peterson, B. M., Ferrarese, L., Gilbert, K. M., et al. 2004, *ApJ*, 613, 682, doi: [10.1086/423269](https://doi.org/10.1086/423269)
- Richards, G. T., Lacy, M., Storrie-Lombardi, L. J., et al. 2006, *ApJS*, 166, 470, doi: [10.1086/506525](https://doi.org/10.1086/506525)
- Różańska, A., & Czerny, B. 2000a, *MNRAS*, 316, 473, doi: [10.1046/j.1365-8711.2000.03429.x](https://doi.org/10.1046/j.1365-8711.2000.03429.x)
- . 2000b, *A&A*, 360, 1170
- Shen, Y., Richards, G. T., Strauss, M. A., et al. 2011, *ApJS*, 194, 45, doi: [10.1088/0067-0049/194/2/45](https://doi.org/10.1088/0067-0049/194/2/45)
- Shen, Y., Greene, J. E., Ho, L. C., et al. 2015, *ApJ*, 805, 96, doi: [10.1088/0004-637X/805/2/96](https://doi.org/10.1088/0004-637X/805/2/96)
- Siemiginowska, A., & Czerny, B. 1989, *MNRAS*, 239, 289, doi: [10.1093/mnras/239.1.289](https://doi.org/10.1093/mnras/239.1.289)
- Sironi, L., & Narayan, R. 2015, *ApJ*, 800, 88, doi: [10.1088/0004-637X/800/2/88](https://doi.org/10.1088/0004-637X/800/2/88)
- Starling, R. L. C., Siemiginowska, A., Uttley, P., & Soria, R. 2004, *MNRAS*, 347, 67, doi: [10.1111/j.1365-2966.2004.07167.x](https://doi.org/10.1111/j.1365-2966.2004.07167.x)
- Taam, R. E., Qiao, E., Liu, B. F., & Meyer-Hofmeister, E. 2018, *ApJ*, 860, 166, doi: [10.3847/1538-4357/aac50d](https://doi.org/10.3847/1538-4357/aac50d)
- Tovmassian, H. M. 2001, *Astronomische Nachrichten*, 322, 87, doi: [10.1002/1521-3994\(200106\)322:2\(87::AID-ASNA87\)3.0.CO;2-S](https://doi.org/10.1002/1521-3994(200106)322:2(87::AID-ASNA87)3.0.CO;2-S)

- Trippe, S. 2015, *Journal of Korean Astronomical Society*, 48, 203, doi: [10.5303/JKAS.2015.48.3.203](https://doi.org/10.5303/JKAS.2015.48.3.203)
- Vestergaard, M., & Peterson, B. M. 2006, *ApJ*, 641, 689, doi: [10.1086/500572](https://doi.org/10.1086/500572)
- Volonteri, M., Sikora, M., Lasota, J.-P., & Merloni, A. 2013, *ApJ*, 775, 94, doi: [10.1088/0004-637X/775/2/94](https://doi.org/10.1088/0004-637X/775/2/94)
- Wandel, A., Peterson, B. M., & Malkan, M. A. 1999, *ApJ*, 526, 579, doi: [10.1086/308017](https://doi.org/10.1086/308017)
- Wang, F., Du, P., Hu, C., et al. 2016, *ApJ*, 824, 149, doi: [10.3847/0004-637X/824/2/149](https://doi.org/10.3847/0004-637X/824/2/149)
- Wang, J.-M., Du, P., Baldwin, J. A., et al. 2012, *ApJ*, 746, 137, doi: [10.1088/0004-637X/746/2/137](https://doi.org/10.1088/0004-637X/746/2/137)
- Wang, J.-M., Du, P., Brotherton, M. S., et al. 2017, *Nature Astronomy*, 1, 775, doi: [10.1038/s41550-017-0264-4](https://doi.org/10.1038/s41550-017-0264-4)
- Wang, J.-M., Du, P., Li, Y.-R., et al. 2014a, *ApJL*, 792, L13, doi: [10.1088/2041-8205/792/1/L13](https://doi.org/10.1088/2041-8205/792/1/L13)
- Wang, J.-M., Qiu, J., Du, P., & Ho, L. C. 2014b, *ApJ*, 797, 65, doi: [10.1088/0004-637X/797/1/65](https://doi.org/10.1088/0004-637X/797/1/65)
- Wang, J.-M., Hu, C., Li, Y.-R., et al. 2009, *ApJL*, 697, L141, doi: [10.1088/0004-637X/697/2/L141](https://doi.org/10.1088/0004-637X/697/2/L141)
- Wang, J.-M., Ge, J.-Q., Hu, C., et al. 2011, *ApJ*, 739, 3, doi: [10.1088/0004-637X/739/1/3](https://doi.org/10.1088/0004-637X/739/1/3)
- Watson, D., Denney, K. D., Vestergaard, M., & Davis, T. M. 2011, *ApJL*, 740, L49, doi: [10.1088/2041-8205/740/2/L49](https://doi.org/10.1088/2041-8205/740/2/L49)
- Yuan, F., & Narayan, R. 2014, *ARA&A*, 52, 529, doi: [10.1146/annurev-astro-082812-141003](https://doi.org/10.1146/annurev-astro-082812-141003)

Table 1. Time delays

Name	$\log L_{5100}$ (erg/s)	$R_{H\beta}$ (ldt)	$\log M_{BH}$ M_{\odot}	L/L_{Edd}	Ref
SDSS J140518	44.33	$41.6^{+14.8}_{-8.3}$	7.74	0.288	1
SDSS J140759	43.58	$16.3^{+13.1}_{-6.6}$	7.67	0.059	
SDSS J140812	43.15	$10.5^{+1.0}_{-2.2}$	7.26	0.058	
SDSS J140904	44.15	$11.6^{+8.6}_{-4.6}$	8.45	0.036	
SDSS J141004	44.22	$53.5^{+4.2}_{-4.0}$	8.32	0.058	
SDSS J141018	43.58	$16.2^{+2.9}_{-4.5}$	7.65	0.063	
SDSS J141031	44.02	$35.8^{+1.1}_{-10.3}$	7.91	0.094	
SDSS J141041	43.82	$21.9^{+4.2}_{-2.4}$	7.85	0.070	
SDSS J141112	44.12	$20.4^{+2.5}_{-2.0}$	7.41	0.375	
SDSS J141115	44.31	$49.1^{+11.1}_{-2.0}$	7.94	0.174	
SDSS J141123	44.13	$13.0^{+1.4}_{-0.8}$	7.38	0.411	
SDSS J141135	44.04	$17.6^{+8.6}_{-7.4}$	7.56	0.224	
SDSS J141147	44.02	$6.4^{+1.5}_{-1.4}$	6.95	0.865	
SDSS J141214	44.40	$21.4^{+4.2}_{-6.4}$	7.26	1.019	
SDSS J141314	44.52	$43.9^{+4.9}_{-4.3}$	9.21	0.015	
SDSS J141318	43.94	$20.0^{+1.1}_{-3.0}$	7.51	0.200	
SDSS J141324	43.94	$25.5^{+10.9}_{-5.8}$	8.92	0.008	
SDSS J141417	43.40	$15.6^{+3.2}_{-5.1}$	8.03	0.017	
SDSS J141532	44.14	$26.5^{+9.9}_{-8.8}$	7.23	0.591	
SDSS J141606	44.80	$32.0^{+11.6}_{-15.5}$	9.07	0.040	
SDSS J141625	43.96	$15.1^{+3.2}_{-4.6}$	7.58	0.178	
SDSS J141645.15	43.21	$5.0^{+1.5}_{-1.4}$	7.93	0.014	
SDSS J141645.58	43.68	$8.5^{+2.5}_{-1.4}$	6.90	0.438	
SDSS J141706	44.19	$10.4^{+6.3}_{-3.0}$	6.70	2.258	
SDSS J141712	43.21	$12.5^{+1.8}_{-2.6}$	8.99	0.001	
SDSS J141724	43.99	$10.1^{+12.5}_{-2.7}$	7.57	0.195	
SDSS J141729	43.29	$5.5^{+5.7}_{-2.1}$	8.28	0.008	
SDSS J141856	45.38	$15.8^{+6.0}_{-1.9}$	8.90	0.224	
SDSS J141859	44.91	$20.4^{+5.6}_{-7.0}$	8.05	0.534	
SDSS J141923	43.12	$11.8^{+0.7}_{-1.5}$	7.18	0.065	
SDSS J141941	44.52	$30.4^{+3.9}_{-8.3}$	7.60	0.612	
SDSS J141952	44.25	$32.9^{+5.6}_{-5.1}$	9.23	0.008	
SDSS J141955	43.40	$10.7^{+5.6}_{-4.4}$	7.69	0.037	
SDSS J142010	44.09	$12.8^{+5.7}_{-4.5}$	8.64	0.021	
SDSS J142023	44.22	$8.5^{+3.2}_{-3.9}$	8.58	0.032	
SDSS J142038	43.46	$25.2^{+4.7}_{-5.7}$	7.67	0.045	
SDSS J142039	44.14	$20.7^{+0.9}_{-3.0}$	7.57	0.275	
SDSS J142043	43.40	$5.9^{+0.4}_{-0.6}$	7.20	0.115	

Table 1 continued

Table 1 (*continued*)

Name	$\log L_{5100}$ (erg/s)	$R_{H\beta}$ (ldt)	$\log M_{BH}$ M_{\odot}	L/L_{Edd}	Ref
SDSS J142049	44.45	$46.0^{+9.5}_{-9.5}$	9.00	0.020	
SDSS J142052	45.06	$11.9^{+1.3}_{-1.0}$	8.73	0.157	
SDSS J142103	43.64	$75.2^{+3.2}_{-3.3}$	7.89	0.041	
SDSS J142112	44.31	$14.2^{+3.7}_{-3.0}$	8.22	0.092	
SDSS J142135	43.47	$3.9^{+0.9}_{-0.9}$	6.60	0.548	
SDSS J142417	44.09	$36.3^{+4.5}_{-5.5}$	7.70	0.180	
Mrk335	43.76	$14.0^{+4.6}_{-3.4}$	6.93	0.501	2
Mrk142	43.59	$6.4^{+7.3}_{-3.4}$	6.47	0.983	
IRASF12397	44.23	$9.7^{+5.5}_{-1.8}$	6.79	2.023	
Mrk486	43.69	$23.7^{+7.5}_{-2.7}$	7.24	0.208	
Mrk382	43.12	$7.5^{+2.9}_{-2.0}$	6.50	0.312	
IRAS04416	44.47	$13.3^{+13.9}_{-1.4}$	6.78	3.577	
MCG06	42.67	$24.0^{+8.4}_{-4.8}$	6.92	0.042	
Mrk493	43.11	$11.6^{+1.2}_{-2.6}$	6.14	0.694	
Mrk1044	43.10	$10.5^{+3.3}_{-2.7}$	6.45	0.322	
SDSS J074352	45.37	$43.9^{+5.2}_{-4.2}$	7.93	2.028	
SDSS J075051	45.33	$66.6^{+18.7}_{-9.9}$	7.67	3.359	
SDSS J075101	44.18	$30.4^{+7.3}_{-5.8}$	7.18	0.733	
SDSS J075949	44.20	$43.9^{+33.1}_{-19.0}$	7.44	0.415	
SDSS J080101	44.27	$8.3^{+9.7}_{-2.7}$	6.78	2.257	
SDSS J080131	43.97	$11.5^{+7.5}_{-3.7}$	6.51	2.121	
SDSS J081441	43.96	$25.3^{+10.4}_{-7.5}$	7.18	0.446	
SDSS J081456	43.99	$24.3^{+7.7}_{-16.4}$	7.44	0.259	
SDSS J083553	44.44	$12.4^{+5.4}_{-5.4}$	6.87	2.722	
SDSS J084533	44.53	$18.1^{+6.0}_{-4.7}$	6.76	4.264	
SDSS J085946	44.41	$34.8^{+9.2}_{-26.3}$	7.30	0.952	
SDSS J093302	44.31	$19.0^{+3.8}_{-4.3}$	7.08	1.245	
SDSS J093922	44.07	$11.9^{+2.1}_{-6.3}$	6.53	2.564	
SDSS J100402	45.52	$32.2^{+43.5}_{-4.2}$	7.44	8.802	
SDSS J101000	44.76	$27.7^{+23.5}_{-7.6}$	7.46	1.456	
SDSS J102339	44.09	$24.9^{+19.8}_{-3.9}$	7.16	0.618	
NGC 5548	43.21	$7.2^{+1.3}_{-0.3}$	7.94	0.014	3
1H 0323+342	43.88	$14.8^{+3.9}_{-2.7}$	7.53	0.164	4
PG0026+129	44.97	$111.0^{+24.1}_{-28.3}$	8.15	0.489	5
PG0052+251	44.81	$89.8^{+24.5}_{-24.1}$	8.64	0.107	
Fairall9	43.98	$17.4^{+3.2}_{-4.3}$	8.09	0.058	
Mrk590	43.50	$25.6^{+6.5}_{-5.3}$	7.55	0.065	
3C120	44.00	$26.2^{+8.7}_{-6.6}$	7.79	0.122	
Ark120	43.87	$39.5^{+8.5}_{-7.8}$	8.47	0.018	
Mrk79	43.68	$15.6^{+5.1}_{-4.9}$	7.84	0.050	

Table 1 continued

Table 1 (*continued*)

Name	$\log L_{5100}$ (erg/s)	$R_{H\beta}$ (ldt)	$\log M_{BH}$ M_{\odot}	L/L_{Edd}	Ref
PG0804+761	44.91	$146.9^{+18.8}_{-18.9}$	8.43	0.223	
Mrk110	43.66	$25.6^{+8.9}_{-7.2}$	7.10	0.265	
PG0953+414	45.19	$150.1^{+21.6}_{-22.6}$	8.44	0.408	
NGC3227	42.24	$3.8^{+0.8}_{-0.8}$	7.09	0.010	
NGC3516	42.79	$11.7^{+1.0}_{-1.5}$	7.82	0.007	
SBS1116+583A	42.14	$2.3^{+0.6}_{-0.5}$	6.78	0.017	
Arp151	42.55	$4.0^{+0.5}_{-0.7}$	6.87	0.035	
NGC3783	42.56	$10.2^{+3.3}_{-2.3}$	7.45	0.009	
Mrk1310	42.29	$3.7^{+0.6}_{-0.6}$	6.62	0.035	
NGC4051	41.90	$2.1^{+0.9}_{-0.7}$	5.72	0.110	
NGC4151	42.09	$6.6^{+1.1}_{-0.8}$	7.72	0.002	
Mrk202	42.26	$3.0^{+1.7}_{-1.1}$	6.11	0.104	
NGC4253	42.57	$6.2^{+1.6}_{-1.2}$	6.49	0.088	
PG1226+023	45.96	$306.8^{+68.5}_{-90.9}$	8.87	0.918	
PG1229+204	43.70	$37.8^{+27.6}_{-15.3}$	8.03	0.034	
NGC4593	42.62	$4.0^{+0.8}_{-0.7}$	7.26	0.017	
NGC4748	42.56	$5.5^{+1.6}_{-2.2}$	6.61	0.064	
PG1307+085	44.85	$105.6^{+36.0}_{-46.6}$	8.72	0.098	
Mrk279	43.71	$16.7^{+3.9}_{-3.9}$	7.97	0.040	
PG1411+442	44.56	$124.3^{+61.0}_{-61.7}$	8.28	0.141	
NGC5548	43.29	$17.6^{+6.4}_{-4.7}$	7.94	0.014	
PG1426+015	44.63	$95.0^{+29.9}_{-37.1}$	8.97	0.033	
Mrk817	43.74	$19.9^{+9.9}_{-6.7}$	7.99	0.042	
Mrk290	43.17	$8.7^{+1.2}_{-1.0}$	7.55	0.031	
PG1613+658	44.77	$40.1^{+15.0}_{-15.2}$	8.81	0.068	
PG1617+175	44.39	$71.5^{+29.6}_{-33.7}$	8.79	0.029	
PG1700+518	45.59	$251.8^{+45.9}_{-38.8}$	8.40	1.137	
3C390.3	44.43	$44.5^{+27.6}_{-17.0}$	9.18	0.013	
NGC6814	42.12	$6.6^{+0.9}_{-0.9}$	7.16	0.007	
Mrk509	44.19	$79.6^{+6.1}_{-5.4}$	8.15	0.081	
PG2130+099	44.20	$9.6^{+1.2}_{-1.2}$	7.05	1.043	
NGC7469	43.51	$10.8^{+3.4}_{-1.3}$	7.60	0.059	
PG1211+143	44.73	$93.8^{+25.6}_{-42.1}$	7.87	0.530	
PG0844+349	44.22	$32.3^{+13.7}_{-13.4}$	7.66	0.265	
NGC5273	41.54	$2.2^{+1.2}_{-1.6}$	7.14	0.002	
KA1858+4850	43.43	$13.5^{+2.0}_{-2.3}$	6.94	0.225	
Mrk1511	43.16	$5.7^{+0.9}_{-0.8}$	7.29	0.055	
MCG6-30-15	41.64	$5.7^{+1.8}_{-1.7}$	6.63	0.008	
UGC06728	41.86	$1.4^{+0.7}_{-0.8}$	5.87	0.073	
MCG+08-11-011	43.33	$15.7^{+0.5}_{-0.5}$	7.72	0.030	

Table 1 continued

Table 1 (*continued*)

Name	$\log L_{5100}$ (erg/s)	$R_{H\beta}$ (ldt)	$\log M_{BH}$ M_{\odot}	L/L_{Edd}	Ref
NGC2617	42.67	$4.3^{+1.1}_{-1.4}$	7.74	0.006	
3C382	43.84	$40.5^{+8.0}_{-3.7}$	8.67	0.011	
Mrk374	43.77	$14.8^{+5.8}_{-3.3}$	7.86	0.061	

NOTE—Ref. 1: Grier et al. (2017), 2: Du et al. (2014, 2015, 2016, 2018), 3: Lu et al. (2016), 4: Wang et al. (2016), 5: Bentz et al. (2013)